

# Effects of Angstrom-Prescott and Hargreaves-Samani Coefficients on Climate Forcing and Solar PV Technology Selection in West Africa

Mfongang Erim Agbor<sup>1</sup>, Sunday O. Udo<sup>1</sup>, Igwe O. Ewona<sup>1,2</sup>, Samuel Chukwujindu Nwokolo<sup>\*1</sup>, Julie C. Ogbulezie<sup>1</sup>, Solomon Okechukwu Amadi<sup>3</sup>, Utibe Akpan Billy<sup>1</sup>

1: Department of Physics, Faculty of Physical Sciences, University of Calabar, Nigeria

2: Department of Physics, Faculty of Physical Sciences, Cross River University of Science and Technology, Nigeria

3: Department of Physics, Faculty of Physical Sciences, Alex Ekwueme Federal University, Ndufu-Alike, Nigeria

Received December 10, 2022; Accepted January 13, 2023; Published January 15, 2023

We evaluated and compared the performance of simulated Angström-Prescott (AP) and Hargreaves-Samani (HS) models on monthly and annual timescales using generalized datasets covering the entire West African region. The fitted AP model yielded more efficient parameters of  $a = 0.366$  and  $b = 0.459$ , whereas the HS model produced a 0.216 coefficient based on an annual timescale, which is more suitable in the region compared to coefficients recommended by the Food and Agriculture Organization (FAO) ( $a = 0.25$  and  $b = 0.5$ ) and HS (0.17), respectively. Employing the FAO and HS recommended coefficients will introduce a relative percentage error (RPE) of 18.388% and 27.19% compared to the RPEs of 0.0014% and 0.1036% obtained in this study, respectively. When considering time and resource availability in the absence of ground-measured datasets, the coefficients obtained in this study can be used for predicting global solar radiation within the region. According to the AP and HS coefficients, the polycrystalline module (p-Si) is more reliable than the monocrystalline module (m-Si) because the p-Si module has a higher tendency to withstand the high temperatures projected to affect the region due to its higher intrinsic properties based on the AP and HS coefficients assessment in the region.

*Keywords:* Ångström-Prescott coefficient; Hargreaves-Samani coefficient; Global solar radiation; Solar PV technologies; Climate forcing

## Introduction

It is undeniable that the growth of solar PV installed capacity in the past years has outpaced the most optimistic projections, as indicated by global cumulative installed capacity at the end of 2013 being only 9.2 MW and worldwide cumulative capacity at year-end 2014 being 15.6 GW [1]. The exponential trend of PV installation growth started in 2008, and the total capacity has doubled every year, with the longest period of increase (since 2009) in 2014, when global installed capacity reached 15.6 GW and year-end solar power share was estimated at 5% of global electricity generation in just 6 years

\*Corresponding authors: henrilynnmfongang@gmail.com (Agbor M.E.); sam31628@gmail.com (Nwokolo S.C.)

(period of 2000-2014), which indicates the steep growth rate in global cumulative installed capacity [1].

The reason for this rapid growth is that in just 6 years, the cost of PV electricity has gone down significantly, which is phenomenal as it was in the years 2007 to 2009 and 2012 to 2014, when global cumulative installed capacity grew by 71% (from 2.1 GW to 3.4 GW) and 47% (from 586 MW to 1.12 GW), respectively [1]. The global cumulative installed capacity of solar power was only 15.6 GW at year-end 2014, and the share of solar power in electricity generation was estimated at 5%. Solar power penetration grew from 20.9 GW in 2010 to 29.3 GW in 2014, with a CAGR (compound annual growth rate) of 60% for the six-year period of 2000-2014. Installed solar capacity in France and Germany amounted to 79 GW and 30 GW [1], respectively, due to a high construction cost and German government subsidies for PV power plants that are only given for the first 15 years of the plants, whereas PV power is available on the commercial grid in countries such as Italy, China, and India for a number of years.

The cost of solar energy is affected by a number of factors. The most important factor is the installation costs of PV cells, particularly photovoltaic modules. The issue of determining the optimal location for a PV power plant has seen a steady decline as the cost of solar cells, per watt, has dropped from \$2.96/W in 1979 to \$1.61/W in 2013 and is expected to drop to about \$1/W by 2016. More than 30 countries in the world are adopting solar power as a part of their national energy mix. After years of investment and research, solar energy has become a reliable source of electricity worldwide, and PV modules are becoming more efficient, using less energy and costing less to produce.

Both of these conditions result in relatively low densities of data regarding incoming solar radiation at the ground level for global climatic information activities, especially at the local level in countries with a few stations in those countries that have started to monitor solar radiation. Satellite observations of solar radiation are more accurate and less expensive than terrestrial observations because they can make use of remote sensing instruments that determine the spectral composition and geographical distribution of incoming solar radiation. Consequently, the density of meteorological stations equipped for measuring solar radiation is too low for global coverage. For instance, there are over 3,000 stations worldwide measuring solar radiation, and in the rest of the world there is a density of about 10 stations per million people [2]. Additionally, a number of statistical problems have been identified, mainly in the field of quantifying solar radiation; for example, the variability of the measurement technique makes it difficult to use solar radiation data for selecting stations to form climatic networks. Finally, spectral solar radiation data on the horizontal and vertical distribution of solar radiation in space can be obtained with high precision, taking advantage of satellite measurements.

Michael FitzGerald has found an equation from the period between 1781 and 1860 that plots monthly mean global solar radiation ( $H$ ) in all sky conditions on the horizontal axis versus  $H$  in clear skies ( $H_{\text{clear}}$ ), which is  $S/S_0$  cited in Kimball [3]. Throughout the year, some astronomers believe that global solar radiation is closely related to or directly proportional to the duration of sunshine. However, others suggest that it is not directly related but that it changes in proportion to the strength of atmospheric transparency, according to the Global Precipitation Climatology Project (GPCP), an assessment of climate change conducted by NASA and other international organizations on the time of the Earth's orbit about the sun.

FitzGerald's equation demonstrated that the relationship between monthly mean global solar radiation (H) and the duration of sunshine (S) varies from year to year and decade to decade between 1781 and 1860. FitzGerald found that there was a stable relationship between solar radiation and cloud cover. However, this was not the case in other periods during the nineteenth century. During the decade before 1840, there was an unstable relationship between solar radiation and cloud cover. The main results for this period show an increase in solar radiation because of an increase in global cloud cover and a decrease in solar radiation by changing the duration of sunshine from one decade to another. Therefore, we can say that FitzGerald's equation is only accurate for the last part of the nineteenth century.

Kimball [3] was the first to discover that FitzGerald's equation view of solar radiation in relation to sunlight is highly correlated with or directly proportional to the length of daylight. Angstrom [4] was the first to mathematically represent Kimball's idea. This was accomplished by relating the monthly mean global solar radiation (H) in all clear sky conditions ( $H_{clear}$ ) to the fraction of sunlight duration ( $S/S_o$ ). As a result, Angstrom [4] claims that the relation can be used to estimate H:

$$\frac{H}{H_{clear}} = 0.25 + 0.75 \left( \frac{S}{S_o} \right) \quad (1)$$

The most recent version of the Angstrom-Prescott model (AP) replaces H with daily average extraterrestrial solar radiation parameters ( $H_o$ ) which Prescott modified [5] and is expressed as:

$$\frac{H}{H_o} = 0.25 + 0.54 \left( \frac{S}{S_o} \right) \quad (2)$$

Environmental variables such as cloud cover, relative humidity, wind, temperature, and precipitation regime can help modify the physical AP model. However, these factors vary between physical and environmental parameters, and their effect is difficult to quantify numerically.

The AP model was developed not only to expand energy applications in response to the need for adequate knowledge of available solar resources, but also to study numerous atmospheric physical parameters in which sunlight scattering, reflections, and diffractions influence the variation of AP coefficients in different parts of the world [6]. Paulescu *et al.* [7] identified two categories of algorithms for predicting solar energy using AP coefficients: (1) prediction of global solar irradiance under a clear sky; and (2) physical fit of clear sky estimates to the current sky state based on sunshine duration measurements.

The authors of this study identified additional aspects that the AP model coefficient could help us evaluate. The coefficient can be quantified for various solar PV technologies suitable for solar energy harvesting by analyzing the atmospheric dynamics of the sum of the AP coefficients (a+b) and taking into account that different solar PV modules have different degrees of ability to withstand extreme temperatures due to the inherent characteristics of the module's solar cell. Polycrystalline silicon (p-Si), for example, is more resistant to high temperatures than monocrystalline silicon (m-Si), activating the production of electricity in places with low temperatures induced by a higher percentage of diffuse components of solar radiation worldwide.

Thus, the amplitude of the AP coefficients (a + b) tells us about the transparency of the sky. Since different solar PV technologies have different intrinsic module characteristics, the conditions of the sky allow us to dictate the type of solar module technology suitable for a specific climatic and geographic environment. The p-Si technology is expected to be used in desert, arid, or semi-arid regions, where the sum of

AP coefficients ( $a + b$ ) exceeds 0.65, because it has higher intrinsic modulus properties to withstand extreme temperatures in such climatic conditions with respect to m-Si. Despite the higher energy production, cost-effectiveness, and wider commercialization of m-Si technology compared to p-Si technology, p-Si is highly recommended when considering the effects of climate change on it.

Extreme temperatures, inherently, cause high wind speeds due to low vapour pressure, resulting in low relative humidity and cloud cover, as well as relatively high sunshine duration and fraction in an open savanna [8], suggesting that as the impact of climate change intensifies, extreme temperatures combined with high wind speeds in such open savanna regions may likely result in damaging the solar cell designed to generate voltage for electrification purposes [9]. Extreme wind speed events, on the other hand, have the potential to destroy or damage the module due to the lack of sufficient wind break in open savanna climate regions. These two factors can cause the modules to degrade faster or introduce cracks in the module, potentially reducing the module's energy productivity.

However, m-Si technology is preferred for regions with a low transparency index, which can also be calculated using AP ( $a + b$ ) coefficients. This will essentially lead to a sharper reduction in global solar radiation and, in some rare cases, in solar PV generation. The longer the PV cells are exposed to low AP ( $a+b$ ) environments, implying a high humidity environment, the steeper the expected performance degradation. This could be due to the high concentration of water vapor in the atmosphere, which often leads to the disintegration of the cavity [10].

Cell interconnect failures or broken cells are often exacerbated in m-Si technology compared to p-Si modules, according to Obiwulu *et al.* [11]. This suggests that a local climate and geographic environment with hot and humid weather (as determined by AP coefficients) may accelerate these deterioration processes, which are common in regions with high relative humidity or a low clarity index (implying a low sum of AP coefficients).

AP coefficients ( $a+b$ ) can also be used to estimate the length of sunlight and clarity index, as well as their implications for climate pressure dynamics and air quality [12]. The Earth's atmosphere is made up of gases, particles, and clouds that form a thin column around the planet. This thin column contains billions of tons of pollutants that change the atmosphere unintentionally. These pollutants are produced by the burning of fossil fuels for energy needs and domestic and industrial transport, as well as forest fires, volcanoes, soil dust, and sea salts. Carbon dioxide, a greenhouse gas, is the final by-product of all forms of combustion [13]. According to Ramanathan and Feng [14], the cumulative effects of these reactions produce ozone, another greenhouse gas that is a major contributor to global warming and climate change.

As a result of the renewable energy and atmospheric benefits of the AP model, countless empirical models based on the AP model and other modified models such as exponential, logarithmic, quadratic, polynomial, and power law models have been introduced worldwide, among others, for the estimation of global solar radiation. This pattern is well documented for Nigeria [15], West Africa [16], Africa [17], India [18], China [19], and the globe [20].

The availability and demand for air temperature input data, which can be easily measured globally, are of particular interest in temperature prediction models. Hargreaves and Samani [21] developed the first temperature-based model for predicting global solar radiation, using maximum and minimum temperatures and extraterrestrial solar radiation

as input parameters, and obtained an empirical coefficient of 0.17, as shown in Equation 3. It has since been recognized as one of the most popular, simple, and accurate temperature models for predicting global solar radiation and can be used for short- and long-term predictions of global solar radiation expressed as:

$$\frac{H}{H_0} = 0.17(\Delta T)^{0.5} \quad (3)$$

where  $H$  is the extraterrestrial solar radiation on a horizontal surface,  $H_0$  is the temperature gradient depicting the difference between the maximum and minimum temperature?

This model has been used by numerous researchers to predict global solar radiation in various parts of the world. However, because of differences in climatic and geographical conditions unique to different locations around the world, the obtained coefficients of 0.17 seem to vary considerably.

When the hours of sunshine datasets needed to evaluate the AP model were not available due to cost, the instrumentation network, or the expertise required for ground-based observations, researchers have often used this approach to primarily generate solar energy data. On the other hand, this study suggests that climate and geographic location-specific Hargreave-Samani adjustment coefficients (AHC) can be used to estimate climate pressure dynamics and air quality in inland and coastal regions. Some investigators reported that the AHS coefficient ranged from 0.19 to 0.21 in coastal regions [22, 23] and fell below this range in inland regions to around 0.17 depending on the local climate and geographical conditions of the sites.

When evaluating their impacts on climate forcing dynamics and air quality in a given location, what does a higher AHC value inland or a lower value in the coastal region imply? The higher AHC value obtained for coastal regions often indicates high cloud cover and relative humidity, which can return additional longwave radiation to the ground, reducing the influence of the air temperature gradient on global solar radiation. This means that the smaller the air temperature gradient, mainly caused by the influence of open water bodies on the atmosphere, the longer the AHC, which can lead to large errors in estimating global solar radiation using the Hargreaves-Samani (HS), and vice versa.

According to atmospheric research, increased or greater values of cloud cover and relative humidity increase diffuse solar radiation and decrease the normal direct radiation available through scattering; at the same time, global solar radiation remains undisturbed. This reduces the amount of conventional direct radiation available that is needed to generate more solar energy for concentrated solar power (CSP). Normal direct solar radiation must be equal to or slightly higher than global solar radiation for concentrated solar power to work effectively [24]. Solar PV technologies, on the other hand, can still be used in this climate. Basically, m-Si technology is recommended for the maximum use of solar energy because its inherent properties favour scattered light over p-Si in places with higher levels of global solar radiation than with normal direct irradiation.

Therefore, the first objective of this paper was to provide AP and HS coefficients in West Africa using generalized datasets that have not been used in the literature since the beginning of solar radiation prediction. In addition, the study proposes a qualitative approach to the analysis of the implications of the AP and HS coefficients for predicting global solar radiation and potential evapotranspiration on climate pressure dynamics, as well as suitable solar PV technology and solar energy concentration in West Africa, which have not been previously implemented in the literature using generalized data sets for the region. Third, the authors proposed an analytical approach based on a rigorous

error metric analysis to determine the predictability of the APC ( $a = 0.25$  and  $b = 0.5$ ) recommended by the Food and Agriculture Organization (FAO) to estimate potential evapotranspiration when no ground observations are available, as well as validation of the AHC's performance for the prediction of global solar radiation in West Africa in this era of climate change and global sustainability, which has been studied in the literature using generalized regression.

## Materials and Methods

### Data Description, Quality and Modeling

Surface downwelling shortwave radiation (hereafter, global solar radiation,  $W/m^2$ ), incident shortwave radiation in the upper atmosphere (hereafter, extraterrestrial,  $W/m^2$ ), total fraction of clouds (%), relative humidity (%), minimum surface air temperature ( $T_{min}$ ) at 2 m height ( $^{\circ}C$ ), maximum cloud air temperature surface ( $T_{max}$ ) at 2 m height ( $^{\circ}C$ ), with monthly spatial resolution were used in this study. These datasets were generated from two different Global Climate Model (GCM) outputs participating in Coupled Model Intercomparison Project Phase 6 (CMIP6). The datasets were downloaded using the latitudes cutting across North ( $28^{\circ}$ ) and South ( $30^{\circ}$ ), as well as the longitudes cutting across the west ( $-28^{\circ}$ ) and east ( $15^{\circ}$ ) of West Africa as a sub-region on the Africa continent under monthly time resolution as shown in Fig. 1. Using a conversion factor of 11.6, the obtained datasets for global solar radiation and extraterrestrial solar radiation in  $W/m^2$  were converted to  $MJ/m^2/d$ . Meteo-solar parameters were used to fit the Anstrom-PreScott [5] and Hargreaves-Samani [21] coefficients to global solar radiation prediction models, as well as to assess the implications of the coefficients on climate forcing dynamics and technology selection for solar photovoltaic in the West African Region.

The two GCMs (National Oceanic and Atmospheric Administration, Geophysical Fluid Dynamics Laboratory, USA (GFDL-ESM4), and National Centre for Meteorological Research, France (HadGEM3-GC31) are chosen based on the availability of relevant energy variables for all selected SSPs developed by the European Centre for Medium Weather Forecasts (ECMWF) (<https://www.ecmwf.int/en/forecasts/datasets/reanalysis-datasets/era5>). Table 1 presents a summary of the GCMs along with their spatiotemporal resolution.

**Table 1.** Summary of two Global Climate Models (GCMs) from Coupled Model Intercomparison Project Phase 6 (CMIP6)

Model	Centre	Grid size (long × lat) /Spatial resolution		Temporal resolution
		Historical	Future	
GFDL-ESM4	National Oceanic and Atmospheric Administration, Geophysical Fluid Dynamics Laboratory	288 × 180 (1.25° × 1.00°)	288 × 180 (1.25° × 1.00°)	Monthly
HadGEM3-GC31	National Centre for Meteorological Research, France	1024 × 768 (0.35° × 0.23°)	432 × 324 (0.83° × 0.55°)	Monthly

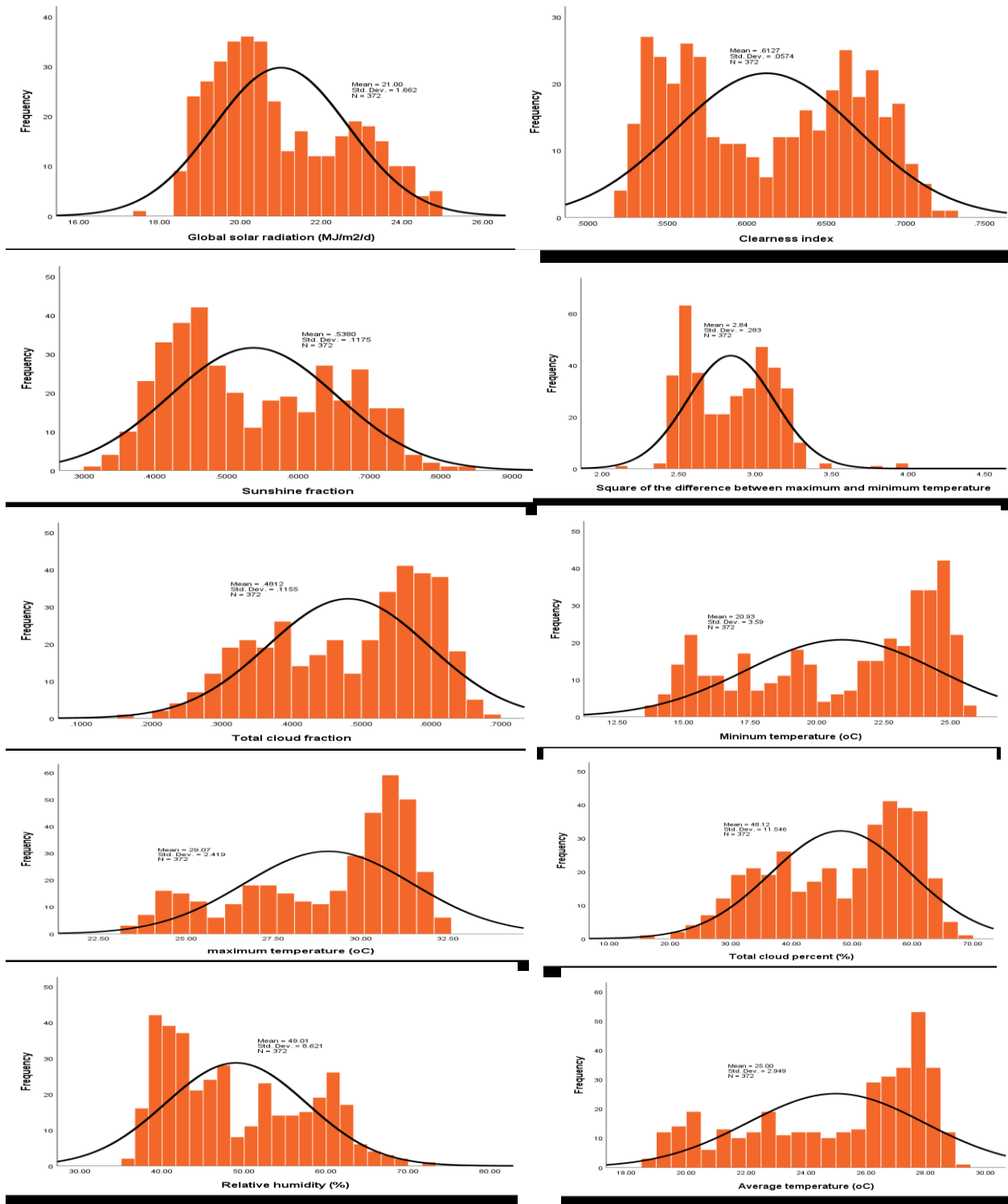


Fig. 1. Descriptive statistics of input and output parameters

Since these two GCM model outputs have different spatial resolutions, they were averaged to reduce the margin of error. The total cloud fraction parameter was used to evaluate the fraction of sunlight in addition to the above parameters, which are used directly to predict global solar radiation. Equation (4) describes the fit of the conventional numerical model using the high-resolution sunshine fraction ( $S/S_o$ ) and total cloud fraction ( $clt$ ) parameters obtained from Zhu *et al.* [25]:

$$S/S_o = 0.946 - 0.6355(clt/100) - 0.4173(clt/100)^2 \quad (4)$$

Khorasanizadeh *et al.* [26] developed a scattering technique to independently confirm the quality of the clearness index and sunshine fraction datasets, respectively, as they were important components of the input settings. The Khorasanizadeh *et al.* [26] method was also used to ensure that the quality of the sunshine fraction was checked. The HadGEM3-GC31 datasets were used to test the developed models using historical data from 1984 to 2014. The GFDL-ESM4 climate datasets were used to simulate global solar radiation models for West Africa. Table 2 displays the descriptive statistics for the input and output parameters.

**Table 2.** Descriptive statistics of the input and output parameters

Parameter	N	Range	Minimum	Maximum	Mean	Std. Deviation
H	372	7.520	17.470	24.980	20.996	1.662
Ho	372	9.690	28.320	38.010	34.497	3.477
kt	372	0.211	0.518	0.730	0.613	0.057
S/So	372	0.507	0.322	0.829	0.538	0.117
$\Delta T$	372	11.200	4.500	15.700	8.139	1.643
$\Delta T_{0.5}$	372	1.840	2.120	3.960	2.839	0.283
Tave	372	10.400	18.600	29.000	24.997	2.949
clt	372	51.300	16.600	67.900	48.122	11.546
RHave	372	36.600	35.400	72.000	49.008	8.621
Tmin	372	12.100	13.750	25.850	20.927	3.590
Tmax	372	9.100	23.350	32.450	29.067	2.419

Where H is the global solar radiation ( $\text{MJ}/\text{m}^2/\text{d}$ ), Ho stands for extraterrestrial solar radiation ( $\text{MJ}/\text{m}^2/\text{d}$ ), kt represents clearness index, S/So represents sunshine fraction,  $\Delta T$  stands for temperature gradient ( $^{\circ}\text{C}$ ), Tave represents average ambient temperature ( $^{\circ}\text{C}$ ), clt represents total cloud percent (%), RHave represents average relative humidity (%), Tmin and Tmax represent minimum and maximum temperature respectively in degrees Celsius

On both the monthly and annual timescales for West Africa, the statistically validated clearness index and sunshine fraction were used to fit the Angstrom-Preseott [5] adjusted model (AP). The temperature gradient and the clearness index parameter were used in West Africa to fit the Hargreaves-Samani [21] adjusted model (AHS) on monthly and annual timescales. Table 3 shows the coefficients of the Angstrom-Preseott [5] adjusted model (AP) and the Hargreaves-Samani [21] adjusted model (AHS).

**Table 3.** The coefficients of the Angstrom-Prescott (AP) and Hargreaves-Samani (HS) and their respective adjusted coefficients in West Africa

Resolution	Angstrom-Prescott (AP) type model		Hargreaves-Samani type model	
	Original AP model	Present study	Original HS model	Present study
January	$\frac{H}{H_o} = 0.25 + 0.50 \left(\frac{S}{S_o}\right)$	$\frac{H}{H_o} = 0.496 + 0.273 \left(\frac{S}{S_o}\right)$	$\frac{H}{H_o} = 0.17(\Delta T)^{0.5}$	$\frac{H}{H_o} = 0.218(\Delta T)^{0.5}$
February	$\frac{H}{H_o} = 0.25 + 0.50 \left(\frac{S}{S_o}\right)$	$\frac{H}{H_o} = 0.475 + 0.304 \left(\frac{S}{S_o}\right)$	$\frac{H}{H_o} = 0.17(\Delta T)^{0.5}$	$\frac{H}{H_o} = 0.214(\Delta T)^{0.5}$
March	$\frac{H}{H_o} = 0.25 + 0.50 \left(\frac{S}{S_o}\right)$	$\frac{H}{H_o} = 0.506 + 0.249 \left(\frac{S}{S_o}\right)$	$\frac{H}{H_o} = 0.17(\Delta T)^{0.5}$	$\frac{H}{H_o} = 0.213(\Delta T)^{0.5}$
April	$\frac{H}{H_o} = 0.25 + 0.50 \left(\frac{S}{S_o}\right)$	$\frac{H}{H_o} = 0.491 + 0.263 \left(\frac{S}{S_o}\right)$	$\frac{H}{H_o} = 0.17(\Delta T)^{0.5}$	$\frac{H}{H_o} = 0.215(\Delta T)^{0.5}$
May	$\frac{H}{H_o} = 0.25 + 0.50 \left(\frac{S}{S_o}\right)$	$\frac{H}{H_o} = 0.436 + 0.343 \left(\frac{S}{S_o}\right)$	$\frac{H}{H_o} = 0.17(\Delta T)^{0.5}$	$\frac{H}{H_o} = 0.214(\Delta T)^{0.5}$
June	$\frac{H}{H_o} = 0.25 + 0.50 \left(\frac{S}{S_o}\right)$	$\frac{H}{H_o} = 0.411 + 0.367 \left(\frac{S}{S_o}\right)$	$\frac{H}{H_o} = 0.17(\Delta T)^{0.5}$	$\frac{H}{H_o} = 0.215(\Delta T)^{0.5}$
July	$\frac{H}{H_o} = 0.25 + 0.50 \left(\frac{S}{S_o}\right)$	$\frac{H}{H_o} = 0.358 + 0.422 \left(\frac{S}{S_o}\right)$	$\frac{H}{H_o} = 0.17(\Delta T)^{0.5}$	$\frac{H}{H_o} = 0.212(\Delta T)^{0.5}$
August	$\frac{H}{H_o} = 0.25 + 0.50 \left(\frac{S}{S_o}\right)$	$\frac{H}{H_o} = 0.346 + 0.437 \left(\frac{S}{S_o}\right)$	$\frac{H}{H_o} = 0.17(\Delta T)^{0.5}$	$\frac{H}{H_o} = 0.215(\Delta T)^{0.5}$
September	$\frac{H}{H_o} = 0.25 + 0.50 \left(\frac{S}{S_o}\right)$	$\frac{H}{H_o} = 0.403 + 0.351 \left(\frac{S}{S_o}\right)$	$\frac{H}{H_o} = 0.17(\Delta T)^{0.5}$	$\frac{H}{H_o} = 0.215(\Delta T)^{0.5}$
October	$\frac{H}{H_o} = 0.25 + 0.50 \left(\frac{S}{S_o}\right)$	$\frac{H}{H_o} = 0.426 + 0.340 \left(\frac{S}{S_o}\right)$	$\frac{H}{H_o} = 0.17(\Delta T)^{0.5}$	$\frac{H}{H_o} = 0.217(\Delta T)^{0.5}$
November	$\frac{H}{H_o} = 0.25 + 0.50 \left(\frac{S}{S_o}\right)$	$\frac{H}{H_o} = 0.437 + 0.342 \left(\frac{S}{S_o}\right)$	$\frac{H}{H_o} = 0.17(\Delta T)^{0.5}$	$\frac{H}{H_o} = 0.223(\Delta T)^{0.5}$
December	$\frac{H}{H_o} = 0.25 + 0.50 \left(\frac{S}{S_o}\right)$	$\frac{H}{H_o} = 0.527 + 0.221 \left(\frac{S}{S_o}\right)$	$\frac{H}{H_o} = 0.17(\Delta T)^{0.5}$	$\frac{H}{H_o} = 0.225(\Delta T)^{0.5}$
Annual	$\frac{H}{H_o} = 0.25 + 0.50 \left(\frac{S}{S_o}\right)$	$\frac{H}{H_o} = 0.366 + 0.459 \left(\frac{S}{S_o}\right)$	$\frac{H}{H_o} = 0.17(\Delta T)^{0.5}$	$\frac{H}{H_o} = 0.216(\Delta T)^{0.5}$

### Analytical Tools and Performance Evaluation

The coefficient of determination (R<sup>2</sup>), root mean square error (RMSE), normalized root mean square error (nRMSE), relative percentage error (RPE), skill score (SS), and mean absolute percentage error (MAPE) were the evaluation metrics used in this study, as shown in Table 4.

**Table 4.** Details of the statistical indicators

S/N	Abbreviation	Statistical test	Expression	Idea value
1.	R <sup>2</sup>	Coefficient of determination	$R^2 = 1 - \left[ \frac{\sum_{i=1}^n (O_i - P_i)^2}{\sum_{i=1}^n (O_i - O_{ave})^2} \right]$	One
2.	RMSE	Root mean square error	$RMSE = \sqrt{\frac{1}{n} \sum_{i=1}^n (O_i - P_i)^2}$	Zero
3.	nRMSE	Normalized root mean square error	$nRMSE = \frac{RMSE}{\sum_{i=1}^n (H)}$	Zero
4.	RPE	Relative percentage error	$RPE = \sum_{i=1}^n \left( \frac{O_i - P_i}{P_i} \right) \times 100$	Zero
5.	SS	Skill score	$SS = 1 - \frac{nRMSE_{present\ study}}{nRMSE_{literature}}$	One
6.	MAPE	Mean absolute percentage error	$MAPE = \frac{1}{n} \sum_{i=1}^n  O_i - P_i  \times 100$	Zero

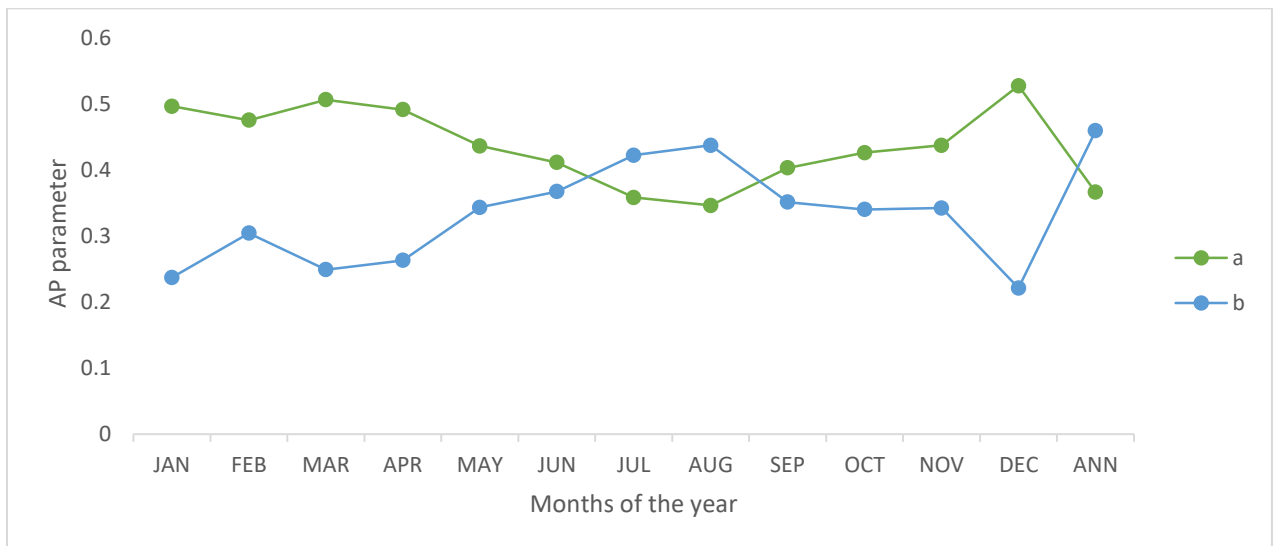
## Results and Discussion

### Performance of AP Parameters in West Africa

According to the statistics of the AP parameter in the different months and according to the annual time scale (Table 3), the parameter a had a higher value in West Africa. The parameter reported a monthly value of 0.346 in August and a monthly value of 0.527 in December, with a corresponding annual value of 0.366. The monthly variability of parameter b was the inverse of that of parameter a, with a maximum value of 0.437 in August and a minimum value of 0.221 in December, and a corresponding annual value of 0.459, which is the maximum value for parameter b. Figure 2 shows that the trend between the AP parameters (a and b) is inverse for daily, monthly, and annual time scale fluctuations. For example, in August, both parameters a and b produced maximum and minimum values. Consequently, the two parameters converge between June and July, August and September, and December and the annual value. Figure 2 shows that the AP parameter gradually increases from January to August and then begins to decrease from September to December, with an accelerated value of 0.459 representing the maximum during the entire monthly period. In contrast, the AP metric decreased gradually from January to August before starting to accelerate from September to December, with a corresponding decrease in value on the annual time scale. Figure 3 shows that the AP a+b parameter produced somewhat uniform values from May to August, with a minimum value in January and a maximum value of 0.783 in August, while the annual time scale value accelerated over the range 0.733–0.779 between January and December to 0.825.

**Table 5.** Variation of AP parameters in West Africa

Month	Present study AP parameters			FAO recommended AP parameters		
	a	b	a+b	a	b	a+b
JAN	0.496	0.237	0.733	0.25	0.5	0.75
FEB	0.475	0.304	0.779	0.25	0.5	0.75
MAR	0.506	0.249	0.755	0.25	0.5	0.75
APR	0.491	0.263	0.754	0.25	0.5	0.75
MAY	0.436	0.343	0.779	0.25	0.5	0.75
JUN	0.411	0.367	0.778	0.25	0.5	0.75
JUL	0.358	0.422	0.78	0.25	0.5	0.75
AUG	0.346	0.437	0.783	0.25	0.5	0.75
SEP	0.403	0.351	0.754	0.25	0.5	0.75
OCT	0.426	0.34	0.766	0.25	0.5	0.75
NOV	0.437	0.342	0.779	0.25	0.5	0.75
DEC	0.527	0.221	0.748	0.25	0.5	0.75
ANN	0.366	0.459	0.825	0.25	0.5	0.75

**Fig. 2.** Variation of AP parameters in West Africa

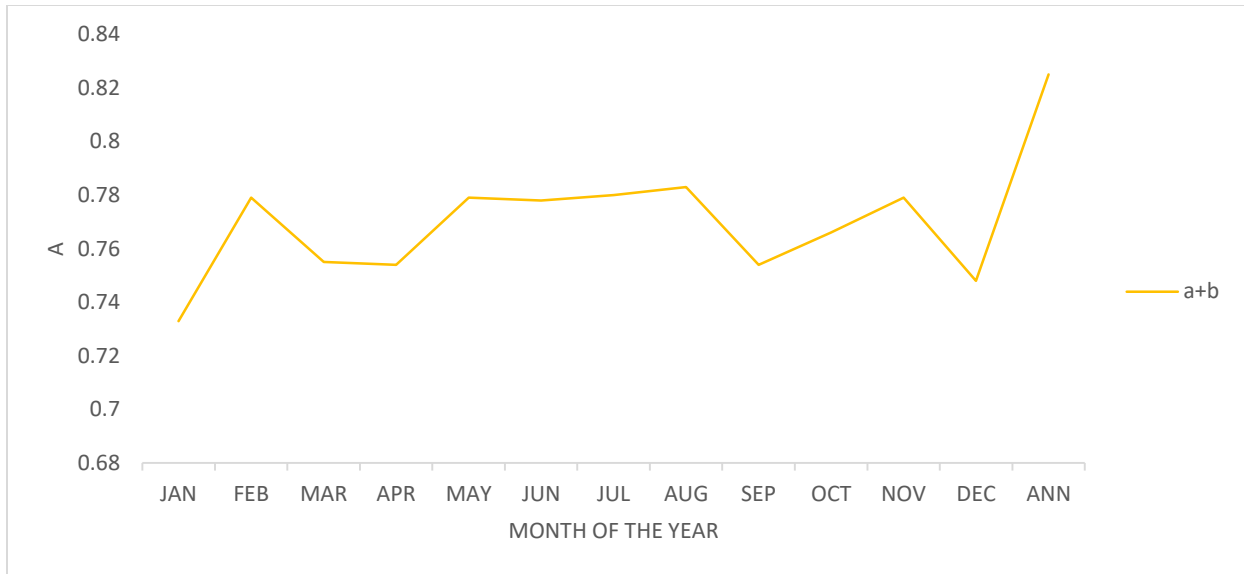


**Fig. 3.** Variation of a+b AP parameter in West Africa

Compared to the FAO parameter values ( $a = 0.25$  and  $b = 0.50$ ), the average parameter "a" in each month as well as the annual value were higher, and the monthly value and the annual value of the "b" parameter were lower. If the recommended FAO values of  $a = 0.25$  and  $b = 0.50$  are used to estimate global solar radiation or potential evaporation, the system will have an additional margin of error of 46.4% and a relative percentage error of -8.2%, according to Table 6. Since the annual value is the lowest, a higher margin of error is introduced on a monthly basis, as shown in Table 6. However, in this era of climate change and global warming, it is clear that the AP parameters proposed by the FAO are not suitable for West Africa, as it will be necessary to estimate the impacts of climate change on solar PV generation, net radiation, net primary productivity, and potential evaporation. these solar flux parameters, introducing an additional margin of error due to the sensitivity of climate change to input and output.

**Table 6.** Error metrics between observed and FAO AP parameters in West Africa

Month/Annual	a				b			
	RMSE	MAPE	nRMSE	RPE	RMSE	MAPE	nRMSE	RPE
JAN	0.0071	0.0413	0.0143	98.4	0.0076	0.0925	0.0320	-52.6
FEB	0.0065	0.0395	0.0137	90.0	0.0057	0.0537	0.0186	-39.2
MAR	0.0074	0.0422	0.0146	102.4	0.0072	0.0840	0.0291	-50.2
APR	0.0070	0.0409	0.0142	96.4	0.0068	0.0751	0.0260	-47.4
MAY	0.0054	0.0356	0.0123	74.4	0.0045	0.0381	0.0132	-31.4
JUN	0.0046	0.0326	0.0113	64.4	0.0038	0.0302	0.0105	-26.6
JUL	0.0031	0.0251	0.0087	43.2	0.0023	0.0154	0.0053	-15.6
AUG	0.0028	0.0231	0.0080	38.4	0.0018	0.0120	0.0042	-12.6
SEP	0.0044	0.0316	0.0110	61.2	0.0043	0.0354	0.0123	-29.8
OCT	0.0051	0.0344	0.0119	70.4	0.0046	0.0392	0.0136	-32.0
NOV	0.0054	0.0357	0.0124	74.8	0.0046	0.0385	0.0133	-31.6
DEC	0.0080	0.0438	0.0152	110.8	0.0081	0.1052	0.0364	-55.8
ANN	0.0033	0.0264	0.0091	46.4	0.0012	0.0074	0.0026	-8.2

Compared to the parameter values ( $a + b = 0.75$ ) provided by FAO, the average parameter  $a + b$  in all months as well as the annual value was higher than expected, with the exception of January and December, which recorded lower values. as shown in Table 5. Using the recommended FAO value of  $a+b = 0.75$  to estimate global solar radiation or potential evaporation will introduce an additional 10.0% margin of error on the annual mean values of the relative percentage error in the system, according to Table 5. The recommended FAO value is overestimated by -2.3% in January and -0.3% in December, according to Table 7, while other parameters introduce marginal errors between 0.5 and 4.5% for the months that are left. Since this annual value is the lowest, a larger margin of error is introduced on a monthly basis, as shown in Table 7. However, in this era of climate change and global warming, it is clear that the AP parameters recommended by FAO56 (the Food and Agriculture Organization (FAO) Irrigation and Drainage Paper No. 56) are inadequate. suitable for West Africa, as these solar flux parameters will be needed to account for the impact of climate change on solar PV generation, net radiation, net primary production, and potential evaporation, which will introduce an additional margin of error due to input and output sensitivity to changing climate.

Multiple results were obtained from adjusting the AP equation coefficient between the adjusted and recommended values. Most of these studies are based on single or multiple stations [27, 28], and provincial or global study regions, as well as uniform coefficient values, are commonly used in regional studies [29, 30, 31]. Although some regional coefficients were interpolated, they were not optimized. Liu *et al.* [32] show that the coefficient "a" ranges from 0.139 to 0.270, with an average of 0.205 in China.

**Table 7.** Error metrics between observed and FAO AP  $a+b$  parameter in West Africa

Month/Annual	a+b			
	RMSE	MAPE	nRMSE	RPE
JAN	0.0005	0.0019	0.0007	-2.3
FEB	0.0008	0.0031	0.0011	3.9
MAR	0.0001	0.0006	0.0002	0.7
APR	0.0001	0.0004	0.0002	0.5
MAY	0.0008	0.0031	0.0011	3.9
JUN	0.0008	0.0030	0.0010	3.7
JUL	0.0009	0.0032	0.0011	4.0
AUG	0.0010	0.0035	0.0012	4.4
SEP	0.0001	0.0004	0.0002	0.5
OCT	0.0005	0.0017	0.0006	2.1
NOV	0.0008	0.0031	0.0011	3.9
DEC	0.0001	0.0002	0.0001	-0.3
ANN	0.0022	0.0076	0.0026	10.0

### Performance of A-P Model for Predicting Global Solar Radiation in West Africa

Table 8 summarizes the performance of global solar radiation prediction on monthly and yearly timescales, as well as training and testing timelines, using FAO-recommended AP parameters and those obtained in this study. The statistical error metric obtained using both approaches revealed that the FAO-recommended AP parameters are ineffective for predicting global solar radiation, whereas those fitted using the parameters in this manner performed significantly better for both the training and training categories. For example, for all 13 models developed between January and December on an annual

time scale, the AP parameters developed in this study yielded upper R2 error metrics ranging from 0.451 to 0.929 and lower R2 error metrics ranging from 0.0011 to 0.0022 for MAPE, between 0.0003 and 0.0008 for nRMSE, 0.0095 and 0.4501 for RPE, and 0.8182 and 0.9167 for skill score values. The skill score error metric is used because the higher the R2 values, the closer they are to one, and the lower the nRMSE values, and the RPE may not fully reveal how accurately predictive performance differs between the FAO-recommended approach and the models adapted in this study.

A skill score error metric indicator was used to compare the performance of the approach used in this study with the one recommended by the FAO. A skill score close to one (between 0.5 and 1) indicates better performance accuracy, while skill scores close to zero and negative values indicate moderate and poor benchmarking results, respectively. Table 8 shows that on an annual time scale, the ability score for all 13 models developed between January and December was between 0.8182 and 0.9167, indicating a lack of predictive ability for the parameters recommended by FAO to assess the potential global solar radiation in West Africa using the AP parameters obtained using the datasets of this study. This may be because the models were built using historical datasets from when global warming had not exceeded 1.0 degree Celsius, compared to the 1.4 degree Celsius reported by the European Center for Medium-Term Weather Forecasts database. beam (ECMWF) in April 2022.

Paulescu *et al.* [33] recently compared the performance of developed AP parameters derived from ground-based data from WRDC and BSRN with four online platforms. The authors found that the performance of platforms using the AP equation is broadly comparable, with ability scores ranging from 6.1% to 40%. They also stated that both platforms and AP parameters are climate-sensitive; however, AP parameters outperformed platforms in tropical and continental climates. The authors also found that no AP equations outperformed the platforms in all seasons and that no platforms outperformed the AP equations in all seasons. According to Paulescu *et al.* [33], there is no recommendation for using a platform or empirical equation. The models developed by the online platform exceeded FAO parameters in this study. Thorough testing of radiometric sources (satellites, reanalyses, empirical equations) against reliable data measured from the ground, as well as dissemination of results, are general requirements for scientific progress in solar radiation modeling and selection of the appropriate model in solar engineering. This would make it easier to compare the results of different scientific studies.

**Table 8.** Performance of Angstrom-Prescott model for estimating global solar radiation in West Africa

Model #		Training Model Fit statistics					Testing Model Fit statistics				
		R2	MAPE	nRMSE	RPE	Skill Score	R2	MAPE	nRMSE	RPE	Skill Score
JAN	Present study	0.729	0.0010	0.0003	0.0095	0.9167	0.663	0.0009	0.0003	0.0086	0.8334
	FAO	0.699	0.0104	0.0036	14.3714	0.0000	0.635	0.0095	0.0033	13.0649	0.0000
FEB	Present study	0.710	0.0013	0.0005	0.4501	0.8718	0.645	0.0012	0.0005	0.4092	0.7925
	FAO	0.709	0.0113	0.0039	15.7238	0.0000	0.645	0.0103	0.0035	14.2944	0.0000
MAR	Present study	0.451	0.0017	0.0006	0.4182	0.8667	0.410	0.0015	0.0005	0.3802	0.7879
	FAO	0.391	0.0131	0.0045	18.7053	0.0000	0.355	0.0119	0.0041	17.0048	0.0000
APR	Present study	0.714	0.0014	0.0005	0.4023	0.9020	0.649	0.0013	0.0005	0.3657	0.8200

	FAO	0.700	0.0147	0.0051	21.5031	0.0000	0.636	0.0134	0.0046	19.5483	0.0000
MAY	Present study	0.851	0.0014	0.0005	0.4015	0.9074	0.774	0.0013	0.0005	0.3650	0.8249
	FAO	0.829	0.0156	0.0054	23.1318	0.0000	0.754	0.0142	0.0049	21.0289	0.0000
JUN	Present study	0.851	0.0015	0.0005	0.3421	0.9074	0.774	0.0014	0.0005	0.3110	0.8249
	FAO	0.562	0.0156	0.0054	23.1274	0.0000	0.511	0.0142	0.0049	21.0249	0.0000
JUL	Present study	0.800	0.0018	0.0006	0.3187	0.8462	0.727	0.0016	0.0005	0.2897	0.7693
	FAO	0.478	0.0112	0.0039	15.6581	0.0000	0.435	0.0102	0.0035	14.2346	0.0000
AUG	Present study	0.792	0.0017	0.0006	0.2955	0.8333	0.720	0.0015	0.0005	0.2686	0.7575
	FAO	0.614	0.0104	0.0036	14.2686	0.0000	0.558	0.0095	0.0033	12.9715	0.0000
SEP	Present study	0.817	0.0017	0.0006	0.2701	0.8696	0.743	0.0015	0.0005	0.2455	0.7905
	FAO	0.726	0.0133	0.0046	19.2397	0.0000	0.660	0.0121	0.0042	17.4906	0.0000
OCT	Present study	0.861	0.0014	0.0005	0.3313	0.9038	0.783	0.0013	0.0005	0.3012	0.8216
	FAO	0.815	0.0149	0.0052	21.9478	0.0000	0.741	0.0135	0.0047	19.9525	0.0000
NOV	Present study	0.929	0.0013	0.0005	0.3886	0.8750	0.845	0.0012	0.0005	0.3533	0.7955
	FAO	0.781	0.0117	0.0040	16.3367	0.0000	0.710	0.0106	0.0036	14.8515	0.0000
DEC	Present study	0.537	0.0013	0.0004	0.4348	0.8919	0.488	0.0012	0.0004	0.3953	0.8108
	FAO	0.509	0.0108	0.0037	15.0118	0.0000	0.463	0.0098	0.0034	13.6471	0.0000
ANN	Present study	0.882	0.0022	0.0008	0.0014	0.8182	0.802	0.0020	0.0007	0.0013	0.7438
	FAO	0.674	0.0128	0.0044	18.3808	0.0000	0.000	0.0000	0.0000	0.0000	0.0000

### Performance of Hargreaves-Samani Model for Predicting Global Solar Radiation

Table 9 summarizes the performance of global solar radiation prediction on monthly and yearly timescales, as well as training and testing timelines, using Hargreaves-Samani (HS) parameter and those obtained in this study. The statistical error metric obtained using both approaches revealed that the HS coefficient is ineffective for predicting global solar radiation, whereas those fitted using the coefficient in this study performed significantly better for both the training and training categories.

A skill score error metric indicator was used to compare the performance of the approach used in this study with the HS. A skill score close to one (between 0.5 and 1) indicates better performance accuracy, while skill scores close to zero and negative values indicate moderate and poor benchmarking results, respectively. Table 9 shows that on an annual time scale, the ability score for all 13 models developed between January and December was between 0.800 to 0.937, indicating a lack of predictive ability for the parameters HS model to assess the potential global solar radiation in West Africa using the datasets of this study. This may be because the models were built using historical datasets from when global warming had not exceeded 1.0 degree Celsius, compared to the 1.4 degree Celsius reported by the European Center for Medium-Term Weather Forecasts database. beam (ECMWF) in April 2022.

**Table 9.** Performance of Hargreaves-Samani model for estimating global solar radiation in West Africa

Model #		Training Model Fit statistics					Testing Model Fit statistics				
		R2	MAPE	nRMSE	RPE	Skill Score	R2	MAPE	nRMSE	RPE	Skill Score
JAN	Present study	0.598	0.0012	0.0004	0.0064	0.937	0.556	0.0011	0.0004	0.0060	0.872
	HS	0.598	0.0183	0.0063	28.2435	0.000	0.556	0.0170	0.0059	26.2730	0.000
FEB	Present study	0.790	0.0016	0.0006	0.8938	0.898	0.735	0.0015	0.0006	0.8314	0.835
	HS	0.800	0.0172	0.0059	25.9703	0.000	0.744	0.0160	0.0055	24.1584	0.000
MAR	Present study	0.917	0.0013	0.0005	0.7001	0.914	0.853	0.0012	0.0005	0.6513	0.850
	HS	0.911	0.0167	0.0058	25.1577	0.000	0.847	0.0155	0.0054	23.4025	0.000
APR	Present study	0.873	0.0018	0.0006	0.7123	0.900	0.812	0.0017	0.0006	0.6626	0.837
	HS	0.877	0.0173	0.0060	26.3106	0.000	0.816	0.0161	0.0056	24.4750	0.000
MAY	Present study	0.799	0.0017	0.0006	0.7975	0.898	0.743	0.0016	0.0006	0.7419	0.835
	HS	0.815	0.0171	0.0059	25.8491	0.000	0.758	0.0159	0.0055	24.0457	0.000
JUN	Present study	0.014	0.0032	0.0011	0.8735	0.825	0.013	0.0030	0.0010	0.8126	0.767
	HS	0.012	0.0182	0.0063	26.5145	0.000	0.011	0.0169	0.0059	24.6647	0.000
JUL	Present study	0.031	0.0034	0.0012	0.7851	0.800	0.029	0.0032	0.0011	0.7303	0.744
	HS	0.030	0.0173	0.0060	24.6948	0.000	0.028	0.0161	0.0056	22.9719	0.000
AUG	Present study	0.203	0.0017	0.0006	0.6952	0.900	0.189	0.0016	0.0006	0.6467	0.837
	HS	0.207	0.0173	0.0060	26.2890	0.000	0.193	0.0161	0.0056	24.4549	0.000
SEP	Present study	0.242	0.0025	0.0009	0.8635	0.852	0.225	0.0023	0.0008	0.8033	0.793
	HS	0.246	0.0175	0.0061	26.5019	0.000	0.229	0.0163	0.0057	24.6529	0.000
OCT	Present study	0.105	0.0032	0.0011	1.0038	0.828	0.098	0.0030	0.0010	0.9338	0.770
	HS	0.108	0.0184	0.0064	27.8204	0.000	0.100	0.0171	0.0060	25.8794	0.000
NOV	Present study	0.358	0.0033	0.0011	0.7425	0.836	0.333	0.0031	0.0010	0.6907	0.778
	HS	0.354	0.0194	0.0067	30.9011	0.000	0.329	0.0180	0.0062	28.7452	0.000
DEC	Present study	0.007	0.0030	0.0010	1.0837	0.857	0.007	0.0028	0.0009	1.0081	0.797
	HS	0.001	0.0202	0.0070	32.4908	0.000	0.001	0.0188	0.0065	30.2240	0.000
ANN	Present study	0.959	0.0020	0.0007	0.1036	0.887	0.892	0.0019	0.0007	0.0964	0.825
	HS	0.959	0.0179	0.0062	27.1905	0.000	0.892	0.0167	0.0058	25.2935	0.000

### Atmospheric Factors Militating the A-P Parameters

The values of parameters a and b, however, can vary from one station to another due to differences in geographical conditions. Therefore, a comprehensive understanding of these parameters is important for accurate estimates of global solar radiation. Therefore, it is crucial to accurately measure parameters a and b in order to properly estimate global solar radiation and further our understanding of regional climatic variations. In particular, the parameter a measures the fraction of radiation reflected by clouds, while the parameter b measures the fraction of radiation transmitted through clouds. This is an important factor because it allows us to determine how much radiation reaches the surface of the Earth and thus affects its climate. By accurately measuring parameters a and b, scientists can better understand how clouds affect the Earth's

radiation budget and how this in turn impacts regional climates. Furthermore, it is also important to understand the effect of aerosols on global solar radiation, as these particles can both absorb and reflect incoming radiation. This can have a significant influence on the Earth's energy balance, and therefore it is essential to take aerosols into account when measuring parameters of  $a$  and  $b$ .

These longwave emissions can interact with other atmospheric gases, such as water vapor and carbon dioxide, creating a complex web of interactions that must be considered when measuring parameters,  $a$  and  $b$ . Thus, a thorough understanding of the interaction between aerosols and radiation is necessary to accurately measure parameters  $a$  and  $b$ . Furthermore, aerosols also influence the albedo of the Earth's surface by increasing its reflectivity. This increased reflectivity reduces the amount of incoming solar radiation, thus affecting the overall climate of a region. Additionally, aerosols can also affect the Earth's radiative budget by absorbing and scattering incoming longwave radiation. This absorption and scattering of longwave radiation can increase or decrease the amount of radiation emitted into space, further contributing to regional climate change.

This leads to a decrease in the amount of solar radiation that is received by the Earth's surface, further altering regional climate. Additionally, the presence of aerosols can also affect precipitation patterns due to their effects on cloud formation and dynamics. By acting as a cloud condensation nucleus, aerosols can result in larger droplets in clouds and increased rain or snowfall. In extreme cases, aerosols can also lead to decreased visibility in the atmosphere, causing reduced levels of photosynthesis and reducing the health of terrestrial ecosystems.

From the experimental results, geographic location, meteorological systems, and atmospheric conditions influenced the parameter values [6, 34, 35]. The astronomical radiant fraction that reaches the Earth's surface on a cloudy day is, according to the literature, influenced by atmospheric conditions such as humidity, dust content, cloud type and thickness, and pollutant concentration [36]. It varies with station altitude [37] and is determined primarily by cloud type and thickness, increasing as cloudiness increases [38]. When the sky is clear, the sum ( $a + b$ ) equals the clarity index, which rises slightly with altitude [39]. The parameter  $b$  represents the transport properties (aerosol density) of a cloudless atmosphere under the influence of altitude and is primarily determined by the atmosphere's total water content and turbidity [40].

Liu *et al.* [31] calibrated AP parameters in China using six classification zones. A partial correlation analysis of the calibration parameters and variables showed that the main influences on the calibration parameters were sunlight duration, temperature, altitude, and precipitation. The authors also found that prediction models accounting for changes in altitude performed better in most regions, suggesting that altitude is the main determinant of AP parameters in most regions of China. The results of Liu *et al.* [31] agree with those of Paulescu *et al.* [33], who showed that height is a necessary input variable for the AP model. According to Liu *et al.* [31], only models of the altitude and precipitation parameters could reliably predict the parameters.

Paulescu *et al.* [7] found that altitude influences  $a$ , and both latitude and altitude influence  $b$ . They demonstrated that the dependence of parameters  $a$  and  $b$  on latitude and longitude was critical to their fit; however, Liu *et al.* [31] unearthed that predictive model 6 did not outperform Chinese predictive models based on altitude. Furthermore, the researchers found no significant correlations between the parameters and latitude or longitude in different parts of China.

## Effects of Angstrom-Prescott Coefficients on Climate Forcing and Solar PV Technology Selection

Solar energy estimators have used the A-P model coefficient "a" to empirically determine the proportion of extraterrestrial solar radiation ( $H_o$ ) in all sky conditions. Under clear sky conditions, the AP model coefficients ( $a + b$ ) were used to calculate the proportion of  $H_o$ . The AP model based on an annual timescale was applied as an example using generalized datasets, that is,

$$\frac{H}{H_o} = 0.366 + 0.459 \left( \frac{S}{S_o} \right) \quad (5)$$

where  $a=0.366$  and  $b=0.459$

On sunny or clear days, solve equation (5) using the methodology of theoretical physics, where  $S = S_o$ , *i.e.*,  $S/S_o = 1$ . The model parameters are changed to  $a+b=0.825$ . This means that under clear sky conditions, approximately 82.5% of extraterrestrial solar radiation ( $H_o$ ) reaches the horizontal surface, while the remaining percentage is absorbed by clouds. On non-sunny days, however,  $S = 0$ , *i.e.*,  $S/S_o = 0$ , and model (5) reduces to a coefficient of 0.366. This means that the clouds absorbed 36.6% of the total available sunlight.

Despite the fact that global solar radiation has three components (namely direct solar radiation, diffuse solar radiation, and reflected solar radiation), the reflected component is often ignored because of its small proportion to the total radiation and the diffuse component. Therefore, most solar meteorological studies consider global solar radiation as a mixture of direct and diffuse components. This means that a greater percentage of the global solar radiation available on the horizontal surface can be attributed to normal direct irradiation on sunny days in West Africa.

According to atmospheric studies, diffuse or diffuse radiation components dominate the available percentage of global solar radiation on non-sunny days (approximately 36.6% according to equation 5). Diffuse light accounts for about 36.6% of global solar radiation on non-sunny days. This means that, compared to a conventional solar module, the use of a monocrystalline (m-Si) solar module with the module's inherent characteristics of trapping and using a higher percentage of available stray light in temperate and humid climates can ensure significantly efficient performance during non-sunny days in the region.

During sunny days, however, a larger percentage of the available global solar radiation (about 82.5% of the total) may be stimulated or produced in a tropical region by normal direct irradiation. This means that the region can experience extreme temperatures due to excess heat being trapped on the horizontal surface for months and days of the year. This could be attributed to clear skies, which allow direct radiation to penetrate easily due to low cloud cover and particulate matter in open savannah, enabling crosswind assessment and purifying air quality. As a result, the weather pressure parameters of clouds and aerosols that attenuate direct solar radiation through scattering and conversion of beam radiation are reduced. As a result, the region is likely to receive high solar fluxes throughout the year except for June-July-August, when the region suffers from a high precipitation regime in most of its southern parts due to open water bodies where increased pressure encourages steam, resulting in high rainfall in those regions. On the other hand, locations in north western Africa will have fewer rainy days and months, as well as longer dry seasons, than locations in the south of the region.

Extreme temperature events, according to the explanation, may be caused by higher tendencies to receive more direct radiation due to the atmosphere opening up as an open savanna region. As a result, the region may require solar PV modules resistant to extreme temperatures to harness the region's abundance of solar radiation, especially in this era of rising global temperatures that are causing climate change and devastating the global environment and economy. This suggests that polycrystalline (p-Si) solar photovoltaic modules suitable for harnessing solar radiation with high-performance capabilities and module resistance to extreme temperatures could be found in the region. According to several literary works, arid, semi-arid and desert locations should use p-Si to harness solar energy fluxes, while humid regions should use m-Si [37, 41, 42]. However, in this era of climate change, the opening up of the atmosphere caused by high clarity index, direct normal irradiance, and low diffuse light, as well as shared socioeconomic pathways caused by low anthropological activity, may not result in increased solar radiation global and ambient temperature. Climate change is caused by a variety of atmospheric forcing factors. Consequently, it is recommended to establish a global climate model in the region accessible through several databases to determine the impacts of climate change on global solar radiation and ambient temperature.

### Effects of Hargreaves-Samani (HS) Coefficient on Climate Forcing and Solar PV Technology Selection

In West Africa, the values of the adjusted coefficient of the Hargreaves-Samani model (HS) are generated using the retrieved datasets described in Section 2.

$$H/H_o = 0.216(\Delta T)^{0.5} \quad (1)$$

$$H/H_o = 0.17(\Delta T)^{0.5} \quad (2)$$

where equation (1) represents adjusted coefficient of Hargreaves-Samani coefficient obtained for West Africa, whereas, equation (2) stands for original coefficient of Hargreaves-Samani model simulated in North America.

This shows that the adjusted Hargreaves-Samani coefficients (AHC) for West Africa is given as 0.216. The value generated in this study is greater than the results reported by other researchers around the world. Allen *et al.* [22] used the ratio of site atmospheric pressure to sea level to estimate the empirical coefficient of the Hargreaves-Samani (HS) model. Allen reported values of 0.17 for inland regions and 0.20 for coastal regions. Hargreaves *et al.* [23] calibrated the HS model and obtained an AHC of 0.16 for inland regions and 0.19 for coastal regions. Adaramola [43] estimated AHC at 0.1945 for the inland region of Akure, Nigeria. For Osogbo, Nigeria, Ohunakin *et al.* [40] found 0.1141. Nwokolo and Ogbulezie [15] found the following values for different parts of Nigeria: Calabar reported an AHC of 0.27, Port Harcourt 0.25, Uyo 0.25, Yenagoa 0.25, Warri 0.25, Asaba 0.23, and Benin City was 0.20, Ikeja was 0.20, and Enugu, Akure, Ilorin, Ibadan, Lokoja, Jos, Bauchi, Gusau, Yola, Kaduna, Maiduguri, and Sokoto were all 0.20. The authors also performed simulations for Kano and Nigeria as a whole. Overall, the authors obtained values of 0.22 and 0.20 for the coastal and interior regions of Nigeria, respectively.

The AHC coefficient obtained in this study is consistent with those reported globally. However, the differences in values from one site to another could be attributed to the fact that global solar radiation is entirely dependent on the local climate and regional geography of the site. However, this high value of 0.216 corresponds to the high values found mainly in coastal regions around the world. Nwokolo and Ogbulezie [15]

reported 0.22 for the coastal region of Nigeria; Allen [22] reported 0.20; and Hargreaves *et al.* [23] reported 0.19 for the coastal region. AHC values should be higher in coastal regions than inland regions, according to numerous experimental results from different parts of the world. This also implies that the smaller the air temperature gradient (difference between maximum and minimum temperature), mainly due to the influence of open bodies of water on the atmosphere, the greater the AHC, which may result in a larger error in estimating global solar radiation (H) from the HS model found in West Africa.

In contrast, the lower AHC obtained in the literature for the interior region is due to a decrease in humidity and cloud cover, which reduces long-wave radiation to the ground, thereby enhancing the effect of air temperature range on global solar radiation, which may cause a lower AHC in the region. This means that the higher the air temperature range, which is primarily caused by decreased humidity, cloud cover, diffuse solar radiation, and so on in the atmosphere, the smaller the AHC, which could improve the HS model's estimation of global solar radiation. For annual values, the AHC value reported in this study is higher than that of the original HS model (0.17).

According to the results, using the original HS model value of 0.17 is grossly inadequate for estimating global solar radiation in West Africa. Rather, a value of 0.216 can improve model performance. However, since the obtained value corresponds to the values of the coastal region as indicated by numerous literature sources [22, 15, 21, 43], an increase in cloudiness, diffuse solar radiation, and humidity, which mainly return additional long-wave radiation to the ground, thus reducing the influence of the air temperature gradient on global solar radiation, is thus expected in the region. This is obvious because the increase in cloud cover, humidity, and diffuse solar radiation, according to various atmospheric researchers, results in a decrease in the direct solar radiation available through the diffusion component of the solar radiation beam, while the solar radiation overall remains constant. However, as global temperatures rise and anthropological activities increase, which is inevitable in a developing region, and more and more additional longwave radiation is added to the ground, global solar radiation is expected to begin to decline rapidly in the near future. While the ambient temperature in the region will rise rapidly. This could lead to a warmer environment, a decrease in global solar radiation potential and normal direct radiation, and an increase in diffuse light. This means that as the global effects of climate change increase, West Africa will become warmer, with a corresponding decrease in global solar and normal direct radiation and an increase in diffuse solar radiation.

In this case, p-Si technology will be the best choice to take advantage of the region's abundant solar energy. This is because, compared to other solar PV modules, the solar technology has higher module intrinsic characteristics to withstand the extreme temperatures of the region. According to Dutta *et al.* [41], solar PV generation will decline in Africa, including North Africa, West Africa, Cameroon, the Republic of the Congo, and the Democratic Republic of the Congo. Photovoltaic and concentrated solar power generation in Africa, North Africa, and West Africa is likely to decline, according to Crook *et al.* [42]. Gaetani *et al.* [44] reduced near-future PV energy availability in Europe and Africa in aerosol-climate modeling experiments. Huber *et al.* [45] investigated the impact of long-term changes in solar radiation projections based on CMIP5 climate models on PV energy yields in Africa and parts of West Africa. According to Zou *et al.* [46], Phase 5 models of a combined intercomparison project in Africa and West Africa showed a reduction in global surface solar radiation and

photovoltaic power. Bazyomo *et al.* [47] showed a decline in PV generation in West Africa, with the exception of Sierra Leone. Fant *et al.* [48] projected small changes in solar PV generation in 2050, with an increase in the winter and a decrease in the summer in most regions of Southern Africa. Patchali *et al.* [49] also reported reductions in global solar radiation at several locations in Togo, West Africa. Ohunakin *et al.* [50] showed a decrease in global solar radiation in Nigeria, with the largest possible decrease in southern Nigeria.

### Effects of Aerosol and Cloud on Climate Forcing

In general, atmospheric aerosols enhance the scattering of radiation from the sun to the ground. Variations in atmospheric properties such as humidity and aerosol concentrations can significantly modify the spectrum of radiation passing through the atmosphere, both by scattering radiation and by absorbing radiation at specific frequencies. This can counteract the greenhouse effect by reflecting back incoming solar radiation, thus cooling the planet. These solar-radiation management techniques have been discussed in the recent literature in connection with a limitation of aerosol efficacy on regional climate [51]. Some earth science programs have begun to study the effects of indirect aerosolization. Aerosol particles play a role in snow formation and the Arctic Sea ice melt. Indirect aerosol effects enhance satellite views of Earth. They could also modify cloud lifetime and cover ocean surfaces, but there is not enough evidence to say that they have that much effect. CO<sub>2</sub> emissions in the atmosphere are a major cause of global warming and have been estimated to have increased over 30% per year on average between 1973 and 2000. Indeed, as the figures show there have been large reductions in sunshine duration during the 20th century. In the light of this, Pope *et al.* [51] observes that the solar radiation does not reach all places on Earth at the same time; atmospheric particulate matter is a key culprit. The dimming or brightening of the atmosphere is caused by air pollution and can be mitigated. The transmittivity of the atmosphere plays a key role in explaining some of the observed changes in global dimming and brightening. Here, the change in the transmittivity of the atmosphere must come from some causes other than climate change, so "changes in the concentration and optical properties of aerosols" will not suffice. Moderate increases in surface cooling, slow surface heating, drying of air and soil, damage to regional circulation systems, reduced removal of pollutants from the atmosphere and the hydrological cycle are all consequences of light pollution. At present, Earth climate is generally warmer than it was over the last two millennia. While current climate models include both effects, they do not include the feedbacks caused by changes in cloud cover. Solar dimming is a form of cloud interference. The most dramatic solar dimming effects, such as those on the African continent, result from volcanic eruptions and fireballs. Solar dimming results from surface cooling, an increase in atmospheric solar heating, a disruption of regional circulation systems, changes in atmospheric thermal structure, suppression of evaporation and precipitation, a slowing down of the hydrological cycle. Depending on the extent of the alterations, there may be changes in ocean circulation and weather patterns that could cause major alterations in the hydrological cycle. Another consequence of changing oceanic currents might be the shifting of continental glaciers, thereby increasing the Earth's albedo. The anticipated changes to the hydrological cycle could be disastrous. Yet existing estimates show that these effects, even if substantial, cannot be the sole cause of climate change at present. The practical implication is that global dimming results in significantly reduced plant growth [52]. Slight and apparently easily resolved, global

dimming may instead have far-reaching effect. Additionally, they play an important role in socialization processes: For instance, they influence the infant's ability to make direct contact with others and its early attachment to the parent. We anticipate that aerosols will pose more hazards as the planet becomes warmer. Salby [53] observes that atmospheric pressure can decrease over a volcanic plume by several millibars. The author, however, concluded the main threat to the earth's climate is the release of sulfuric acid aerosols by volcanoes. He also argues that when volcanic eruptions release particles into the atmosphere, they cool down the troposphere and thus slow global warming. In the mid-nineteenth century, dust particles originating in Asian deserts accumulated over Europe and Northern America, causing violent storms that produced both summer and winter droughts. Contrary to Salby's assertions, it is well known that volcanic eruptions affect climate change. These aerosols serve as scavengers, with the effect of allowing a residual layer to exist at the interface between air and water. For example, large volcanic eruptions and such fluctuations in the content of atmospheric aerosols affect how aerosols are transported to different regions of the atmosphere [54]. The increasing frequency of ash emissions observed since the start of the twentieth century coincides with a significant cooling of the Earth's climate. Over time, aerosols (large particles and droplets in the atmosphere) play an important role in climate fluctuations. Scientists have studied the albedo effect and aerosols for centuries, but this novel provides a very human look at the result of increased emissions. Earth's climate fluctuates rapidly, because the net radiation to Earth is altered by the sun's light and heat output. One of the most important roles that aerosols play in climate change is to scatter sunlight, which is an essential aspect of the general circulation process. Besides also reflecting the influences of global climate change, volcanic eruptions may lead to an increase in ozone depletion [55] and an overall decrease in cloudiness and dimming of sunshine at earth's surface. Thus, the anthropogenic emissions of aerosols impact climate changes [56]. The variable equilibrium constants ( $K$ ) of some phase changes tend to decrease with increased concentrations of aerosols [57]. The moisture content, cloud liquid water content, and latent heat storage characteristics of the atmosphere show a consistent response to aerosol increases [58]. When the albedo effect is balanced by aerosol absorption of incoming radiation, this causes the net cooling effect in polar areas.

### Effects of Cloud and Aerosols on Air Quality

One interpretation of this plot idea is that the climate forcing effects of aerosols and clouds influence air quality through the following processes and mechanisms: causing small but significant changes in ventilation rates; precipitation scavenging; changes in chemical production and loss rates; and dry deposition. In the earlier studies, the ozone concentration had a low sensitivity to temperature (2 to 3.7 times less) than had been observed for PM10 [non-particulate matter] and black carbon. The researchers found that ozone is strongly associated with temperature, as ozone concentrations in both warm and cold years decrease and increase, respectively. Since the date at which the temperature of the Earth's atmosphere began to rise, it has increased annually by 0.85 K. The warming that results from the burning of fossil fuels has major implications for the chemical composition of ozone, a pollutant of considerable concern for public health. Although it was previously known that ozone was dependent on temperature and altitude, the findings from this study were remarkable. Ozone is a reactive, unstable chemical formed from oxygen molecules when ultraviolet light from the sun hits ground level pollutants. Ozone is a molecule that consists of three oxygen atoms bound together in a

molecule that resembles an H. A new study [60] published recently showed that temperature correlated with ozone and water vapor in the atmosphere over land. An increasing number of studies suggest that an increase in temperature is the main cause of this ozone depletion. From 1940 to 1976, the earth was cooler, and during this time there were three times as many days when the minimum overlying ozone concentration fell below 0.12 parts per billion (ppb). The best correlation, from which the present-day figure of 0.84 is derived, occurs between ozone and temperature in the lower atmosphere. Therefore, according to the authors, ozone forms when warmer air near the surface moves upward toward cooler layers of air. Today, this knowledge has helped us make considerable progress in reducing stratospheric ozone depletion, which would eventually lead to a significant reduction of ultraviolet radiation reaching the Earth's surface. Ozone and high temperatures are examples of a positive autocorrelation because ozone is sensitive to changing temperature and higher temperatures lead to more ozone, in spite of the fact that these variables have no direct causal relationship. Ozone is a poisonous gas, found in the atmosphere and emitted by some industrial emissions and forest fires. Large numbers of ozone molecules can be created when sunlight breaks apart ozone molecules with oxygen atoms (ozone is comprised of two oxygen atoms). Ozone affects temperatures through absorption of infrared radiation by liquid water, which returns the energy to space as long as it remains liquid.

Ozone production occurs in the stratosphere as well, where the ionization of water molecules by solar ultraviolet radiation (UV) reduces the reactive hydroxyl radical. Most of these NMVOCs are harmful to the ozone layer and produce secondary organic aerosols (SOAs) [59]. As the concentrations of NMVOCs and NO<sub>x</sub> in the atmosphere rise due to anthropogenic climate change, ozone levels are expected to increase [60]. Ozone is produced in the troposphere by the photochemical oxidation of carbon monoxide (CO), methane and non-methane volatile organic compounds (NMVOCs), and the hydroxyl radical in the presence of reactive nitrogen oxides.

## CONCLUSIONS

The effects of the Angstrom-Prescott [5] and Hargreaves-Samani [21] coefficients on climate forcing and solar PV technology selection in West Africa were studied using monthly averaging datasets. The main finding was that the Angstrom-Prescott and Hargreaves-Samani coefficients are ineffective for assessing global solar radiation over West Africa. On the other hand, coefficients fitted in this study were more efficient for calculating the Angstrom-Prescott and Hargreaves-Samani coefficients in the region. Consequently, if global solar radiation ground measurement datasets were not available in West Africa, the following models based on sunlight and temperature could be used:

$$\frac{H}{H_o} = 0.366 + 0.459 \left( \frac{S}{S_o} \right) \quad (6)$$

$$\frac{H}{H_o} = 0.216(\Delta T)^{0.5} \quad (7)$$

According to the above equation, AP parameters obtained on an annual basis include  $a = 0.366$  and  $b = 0.459$ , whereas the Hargreaves-Samani coefficient of 0.216 can be used as more accurate parameters than the FAO-recommended  $a = 0.25$  and  $b = 0.5$ , as well as the 0.17 recommended by Hargreaves and Samani [21]. The effects of the Angstrom-Prescott and Hargreaves-Samani coefficients were also examined to determine the best solar PV model for West Africa. According to the parameters of the Angstrom-Prescott and Hargreaves-Samani coefficients, the p-Si module is more reliable than the

m-Si module, because the p-Si module has a higher tendency to withstand the high temperatures projected to affect the region due to its higher module intrinsic properties [61].

## ACKNOWLEDGMENTS

The authors would like to acknowledge the European Centre for Medium Weather Forecasts (ECMWF) for providing the data used in this study.

## REFERENCES

- [1] Beiter, P. C., Vincent, N. M., and Ma, O. (2018). *2016 Renewable Energy Grid Integration Data Book* (No. NREL/BK-6A20-71151). National Renewable Energy Lab.(NREL), Golden, CO (United States).
- [2] Benatallah, M., Bailek, N., Bouchouicha, K., Sharifi, A., Abdel-Hadi, Y., Nwokolo, S., S. Band, S., Jamil, B., Mosavi, A., and El-kenawy, E.-S. (2022). Exploring the ability of hybrid extreme machine-based methods to predict solar radiation-a case study of Sahara middle South, Algeria. *NRIAG Journal of Astronomy and Geophysics*.
- [3] Kimball, H. H. (1919). Variations in the total and luminous solar radiation with geographical position in the United States. *Monthly Weather Review*, 47(11), 769-793. DOI: [https://doi.org/10.1175/1520-0493\(1919\)47<769:vittal>2.0.co;2](https://doi.org/10.1175/1520-0493(1919)47<769:vittal>2.0.co;2)
- [4] Angstrom, A. (1924). Solar and terrestrial radiation. Report to the international commission for solar research on actinometric investigations of solar and atmospheric radiation. 50(210), 121-126. DOI: <https://doi.org/10.1002/qj.49705021008>
- [5] Prescott, J. (1940). Evaporation from Water Surface in Relation to Solar Radiation. *Trans R Soc South Aust*, 64,114–118.
- [6] Nwokolo, S. C., Amadi, S. O., Obiwulu, A. U., Ogbulezie, J. C., and Eyibio, E. E. (2022). Prediction of global solar radiation potential for sustainable and cleaner energy generation using improved Angstrom-Prescott and Gumbel probabilistic models. *Cleaner Engineering and Technology*, 6, 100416. DOI: <https://doi.org/10.1016/j.clet.2022.100416>
- [7] Paulescu, M., Stefu, N., Calinoiu, D., Paulescu, E., Pop, N., Boata, R., and Mares, O. (2016). Ångström–Prescott equation: Physical basis, empirical models and sensitivity analysis. *Renewable and Sustainable Energy Reviews*, 62, 495-506.
- [8] Nwokolo, S. C., Obiwulu, A. U., Ogbulezie, J. C., and Amadi, S. O. (2022). Hybridization of statistical machine learning and numerical models for improving beam, diffuse and global solar radiation prediction. *Cleaner Engineering and Technology*, 9, 100529. DOI: <https://doi.org/10.1016/j.clet.2022.100529>
- [9] Obiwulu, A. U., Erusiafe, N., Olopade, M. A., and Nwokolo, S. C. (2022). Modeling and estimation of the optimal tilt angle, maximum incident solar radiation, and global radiation index of the photovoltaic system. *Heliyon*, 8(6). DOI:

- 10.1016/j.heliyon.2022.e09598
- [10] Obiwulu, A. U., Chendo, M. A. C., Erusiafe, N., and Nwokolo, S. C. (2020). Implicit meteorological parameter-based empirical models for estimating back temperature solar modules under varying tilt-angles in Lagos, Nigeria. *Renewable Energy*, 145, 442-457. DOI: <https://doi.org/10.1016/j.renene.2019.05.136>
- [11] Obiwulu, A. U., Erusiafe, N., Olopade, M. A., and Nwokolo, S. C. (2020). Modeling and optimization of back temperature models of mono-crystalline silicon modules with special focus on the effect of meteorological and geographical parameters on PV performance. *Renewable Energy*, 154, 404-431. DOI: <https://doi.org/10.1016/j.renene.2020.02.103>
- [12] Amadi, S. O., Dike, T., and Nwokolo, S. C. (2020). Global Solar Radiation Characteristics at Calabar and Port Harcourt Cities in Nigeria. *Trends in Renewable Energy*, 6(2), 111-130. DOI: <https://doi.org/10.17737/tre.2020.6.2.00114>
- [13] Nwokolo, S. C., Ogbulezie, J. C., and Obiwulu, A. U. (2022). Impacts of climate change and meteo-solar parameters on photosynthetically active radiation prediction using hybrid machine learning with Physics-based models. *Advances in Space Research*, 70(11), 3614-3637. DOI: <https://doi.org/10.1016/j.asr.2022.08.010>
- [14] Ramanathan, V., and Feng, Y. (2009). Air pollution, greenhouse gases and climate change: Global and regional perspectives. *Atmospheric Environment*, 43(1), 37-50. DOI: <https://doi.org/10.1016/j.atmosenv.2008.09.063>
- [15] Nwokolo, S.C., and Ogbulezie, J.C. (2017). A single hybrid parameter-based model for calibrating hargreaves-samani coefficient in Nigeria. *Int J Phys Res* 5(2), 49. DOI: <https://doi.org/10.14419/ijpr.v5i2.8042>
- [16] Nwokolo, S.C., and Ogbulezie, J.C. (2018). A quantitative review and classification of empirical models for predicting global solar radiation in West Africa. *Beni-Suef Univ J Basic Appl Sci*, 7,367–396. DOI: <https://doi.org/10.1016/j.bjbas.2017.05.001>
- [17] Nwokolo, S.C. (2017). A comprehensive review of empirical models for estimating global solar radiation in Africa. *Renew Sustain Energy Rev*, 78, 955–995. DOI: <https://doi.org/10.1016/j.rser.2017.04.101>
- [18] Makade, R. G., Chakrabarti, S., and Jamil, B. (2021). Development of global solar radiation models: A comprehensive review and statistical analysis for Indian regions. *Journal of Cleaner Production*, 293, 126208. DOI: <https://doi.org/10.1016/j.jclepro.2021.126208>
- [19] Gouda, S. G., Hussein, Z., Luo, S., and Yuan, Q. (2020). Review of empirical solar radiation models for estimating global solar radiation of various climate zones of China. 44(2), 168-188. DOI: <https://doi.org/10.1177/0309133319867213>
- [20] Almorox, J., Voyant, C., Bailek, N., Kuriqi, A., and Arnaldo, J. A. (2021). Total solar irradiance's effect on the performance of empirical models for estimating global solar radiation: An empirical-based review. *Energy*, 236, 121486. DOI: <https://doi.org/10.1016/j.energy.2021.121486>
- [21] Hargreaves, G. H., and Samani, Z. A. (1982). Estimating potential evapotranspiration. *Journal of the irrigation and Drainage Division*, 108(3), 225-230. DOI: <https://doi.org/10.1061/taceat.0008673>
- [22] Allen, R. G., Pereira, L. S., Raes, D., and Smith, M. (1998). Crop

- evapotranspiration-Guidelines for computing crop water requirements-FAO Irrigation and drainage paper 56. *Fao, Rome, 300*(9), D05109.
- [23] Hargreaves, G. L., Hargreaves, G. H., and Riley, J. P. (1985). Irrigation Water Requirements for Senegal River Basin. 111(3), 265-275. DOI: doi:10.1061/(ASCE)0733-9437(1985)111:3(265)
- [24] Nwokolo, S.C. and Otse, C.Q. (2019). Impact of Sunshine Duration and Clearness Index on Diffuse Solar Radiation Estimation in Mountainous Climate. *Trends in Renewable Energy*, 5, 307-332. DOI: 10.17737/tre.2019.5.3.00107
- [25] Zhu, W., Wu, B., Yan, N., Ma, Z., Wang, L., Liu, W., Xing, Q., and Xu, J. (2019). Estimating sunshine duration using hourly total cloud amount data from a geostationary meteorological satellite. *Atmosphere*, 11(1), 26. DOI: https://doi.org/10.3390/ATMOS11010026
- [26] Khorasanizadeh, H., and Mohammadi, K. (2016). Diffuse solar radiation on a horizontal surface: Reviewing and categorizing the empirical models. *Renewable and Sustainable Energy Reviews*, 53, 338-362. DOI: https://doi.org/10.1016/j.rser.2015.08.037
- [27] Besharat, F., Dehghan, A. A., and Faghih, A. R. (2013). Empirical models for estimating global solar radiation: A review and case study. *Renewable and Sustainable Energy Reviews*, 21, 798-821. DOI: https://doi.org/10.1016/j.rser.2012.12.043
- [28] Liu, Y., Zhou, Y., Chen, Y., Wang, D., Wang, Y., and Zhu, Y. (2020). Comparison of support vector machine and copula-based nonlinear quantile regression for estimating the daily diffuse solar radiation: A case study in China. *Renewable Energy*, 146, 1101-1112. DOI: https://doi.org/10.1016/j.renene.2019.07.053
- [29] Govindasamy, T. R., and Chetty, N. (2021). Machine learning models to quantify the influence of PM10 aerosol concentration on global solar radiation prediction in South Africa. *Cleaner Engineering and Technology*, 2, 100042. DOI: https://doi.org/10.1016/j.clet.2021.100042
- [30] Li, M.-F., Fan, L., Liu, H.-B., Guo, P.-T., and Wu, W. (2013). A general model for estimation of daily global solar radiation using air temperatures and site geographic parameters in Southwest China. *Journal of Atmospheric and Solar-Terrestrial Physics*, 92, 145-150. DOI: https://doi.org/10.1016/j.jastp.2012.11.001
- [31] Liu, Y., Zhou, Y., Wang, D., Wang, Y., Li, Y., and Zhu, Y. (2018). Reply to “Comments on [“Classification of solar radiation zones and general models for estimating the daily global solar radiation on horizontal surfaces in China”][Energy Convers. Manage. 154 (2017) 168–179] by Liu et al.]. *Energy Conversion and Management*, 168, 653-654.
- [32] Liu, Y., Tan, Q., and Pan, T. (2019). Determining the parameters of the Ångström-Prescott model for estimating solar radiation in different regions of China: Calibration and modeling. *Earth and Space Science*, 6(10), 1976-1986. DOI: https://doi.org/10.1029/2019EA000635
- [33] Paulescu, M., Badescu, V., Budea, S., and Dumitrescu, A. (2022). Empirical sunshine-based models vs online estimators for solar resources. *Renewable and Sustainable Energy Reviews*, 168, 112868. DOI:

- <https://doi.org/10.1016/j.rser.2022.112868>
- [34] Almorox, J., Hontoria, C., and Benito, M. (2011). Models for obtaining daily global solar radiation with measured air temperature data in Madrid (Spain). *Applied Energy*, 88(5), 1703-1709. DOI: <https://doi.org/10.1016/j.apenergy.2010.11.003>
- [35] Chen, R., Ersi, K., Yang, J., Lu, S., and Zhao, W. (2004). Validation of five global radiation models with measured daily data in China. *Energy Conversion and Management*, 45(11), 1759-1769. DOI: <https://doi.org/10.1016/j.enconman.2003.09.019>
- [36] de Barros Silva, A. W., Freitas, B. B., de Alencar Filho, C. L., de Freitas, C. D., de Sousa Junior, E. A., de Castro, E. S., de Araújo, E.M., Correia, F.I.F., da Silva, F.R.P., de Souza, J.J.S., and Martins, L.L.A.P. (2022). Methodology Based on Artificial Neural Networks for Hourly Forecasting of PV Plants Generation. *IEEE Latin America Transactions*, 20(4), 659-668. DOI: <https://doi.org/10.1109/TLA.2022.9675472>
- [37] Nwokolo, S.C., Obiwulu, A.U., and Ogbulezie, J.C. (2023). Machine learning and analytical model hybridization to assess the impact of climate. *Phys Chem Earth*, (In press)
- [38] Hassan, M. A., Bailek, N., Bouchouicha, K., and Nwokolo, S. C. (2021). Ultra-short-term exogenous forecasting of photovoltaic power production using genetically optimized non-linear auto-regressive recurrent neural networks. *Renewable Energy*, 171, 191-209. DOI: <https://doi.org/10.1016/j.renene.2021.02.103>
- [39] Hassan, M. A., Bailek, N., Bouchouicha, K., Ibrahim, A., Jamil, B., Kuriqi, A., Nwokolo, S. C., and El-kenawy, E.-S. M. (2022). Evaluation of energy extraction of PV systems affected by environmental factors under real outdoor conditions. *Theoretical and Applied Climatology*, 150(1), 715-729. DOI: 10.1007/s00704-022-04166-6
- [40] Ohunakin, O. S., Adaramola, M. S., Oyewola, O. M., and Fagbenle, R. O. (2013). Correlations for estimating solar radiation using sunshine hours and temperature measurement in Osogbo, Osun State, Nigeria. *Frontiers in Energy*, 7(2), 214-222. DOI: 10.1007/s11708-013-0241-2
- [41] Dutta, R., Chanda, K., and Maity, R. (2022). Future of solar energy potential in a changing climate across the world: A CMIP6 multi-model ensemble analysis. *Renewable Energy*, 188, 819-829. DOI: <https://doi.org/10.1016/j.renene.2022.02.023>
- [42] Crook, J. A., Jones, L. A., Forster, P. M., and Crook, R. (2011). Climate change impacts on future photovoltaic and concentrated solar power energy output. *Energy & Environmental Science*, 4(9), 3101-3109. DOI: <https://doi.org/10.1039/c1ee01495a>
- [43] Adaramola, M. S. (2012). Estimating global solar radiation using common meteorological data in Akure, Nigeria. *Renewable Energy*, 47, 38-44. DOI: <https://doi.org/10.1016/j.renene.2012.04.005>
- [44] Gaetani, M., Huld, T., Vignati, E., Monforti-Ferrario, F., Dosio, A., and Raes, F. (2014). The near future availability of photovoltaic energy in Europe and Africa in

- climate-aerosol modeling experiments. *Renewable and Sustainable Energy Reviews*, 38, 706-716. DOI: <https://doi.org/10.1016/j.rser.2014.07.041>
- [45] Huber, I., Bugliaro, L., Ponater, M., Garny, H., Emde, C., and Mayer, B. (2016). Do climate models project changes in solar resources? *Solar Energy*, 129, 65-84. DOI: <https://doi.org/10.1016/j.solener.2015.12.016>
- [46] Zou, L., Wang, L., Li, J., Lu, Y., Gong, W., and Niu, Y. (2019). Global surface solar radiation and photovoltaic power from Coupled Model Intercomparison Project Phase 5 climate models. *Journal of Cleaner Production*, 224, 304-324. DOI: <https://doi.org/10.1016/j.jclepro.2019.03.268>
- [47] Bazyomo, S. D. Y. B., Lawin, E. A., Coulibaly, O., and Ouedraogo, A. (2016). Forecasted changes in West Africa photovoltaic energy output by 2045. *Climate*, 4(4), 53. DOI: <https://doi.org/10.3390/cli4040053>
- [48] Fant, C., Adam Schlosser, C., and Strzepek, K. (2016). The impact of climate change on wind and solar resources in southern Africa. *Applied Energy*, 161, 556-564. DOI: <https://doi.org/10.1016/j.apenergy.2015.03.042>
- [49] Patchali, T. E., Ajide, O. O., Matthew, O. J., Salau, T. A. O., and Oyewola, O. M. (2020). Examination of potential impacts of future climate change on solar radiation in Togo, West Africa. *SN Applied Sciences*, 2(12), 1941. DOI: <https://doi.org/10.1007/s42452-020-03738-3>
- [50] Ohunakin, O. S., Adaramola, M. S., Oyewola, O. M., Matthew, O. J., and Fagbenle, R. O. (2015). The effect of climate change on solar radiation in Nigeria. *Solar Energy*, 116, 272-286. DOI: <https://doi.org/10.1016/j.solener.2015.03.027>
- [51] Pope, F. D., Braesicke, P., Grainger, R. G., Kalberer, M., Watson, I. M., Davidson, P. J., and Cox, R. A. (2012). Stratospheric aerosol particles and solar-radiation management. *Nature Climate Change*, 2(10), 713-719.
- [52] Amadi, S. O., and Udo, S. O. (2018). A Study of Multi-Annual Variability of Effective Sunshine Duration in Nigeria and Its Implications for Climate Forcing and Air Quality. *Journal of Health and Environmental Studies*, 2(2), 13-30.
- [53] Salby, M. L. (2012). *Physics of the Atmosphere and Climate*. Cambridge University Press.
- [54] Viana, M., Pey, J., Querol, X., Alastuey, A., de Leeuw, F., and Lükewille, A. (2014). Natural sources of atmospheric aerosols influencing air quality across Europe. *Science of The Total Environment*, 472, 825-833. DOI: <https://doi.org/10.1016/j.scitotenv.2013.11.140>
- [55] Bais, A. F., McKenzie, R. L., Bernhard, G., Aucamp, P. J., Ilyas, M., Madronich, S., & Tourpali, K. (2015). Ozone depletion and climate change: impacts on UV radiation. *Photochemical & Photobiological Sciences*, 14(1), 19-52.
- [56] Levy II, H., Horowitz, L. W., Schwarzkopf, M. D., Ming, Y., Golaz, J.-C., Naik, V., and Ramaswamy, V. (2013). The roles of aerosol direct and indirect effects in past and future climate change. 118(10), 4521-4532. DOI: <https://doi.org/10.1002/jgrd.50192>
- [57] Adams, P. J., Seinfeld, J. H., and Koch, D. M. (1999). Global concentrations of tropospheric sulfate, nitrate, and ammonium aerosol simulated in a general circulation model. 104(D11), 13791-13823. DOI:

<https://doi.org/10.1029/1999JD900083>

- [58] Senf, F., Quaas, J., and Tegen, I. (2021). Absorbing aerosol decreases cloud cover in cloud-resolving simulations over Germany. 147(741), 4083-4100. DOI: <https://doi.org/10.1002/qj.4169>
- [59] Wu, D., Ding, X., Li, Q., Sun, J., Huang, C., Yao, L., Wang, X., Ye, X., Chen, Y., He, H., and Chen, J. (2019). Pollutants emitted from typical Chinese vessels: Potential contributions to ozone and secondary organic aerosols. *Journal of Cleaner Production*, 238, 117862. DOI: <https://doi.org/10.1016/j.jclepro.2019.117862>
- [60] Fu, T. M., & Tian, H. (2019). Climate change penalty to ozone air quality: review of current understandings and knowledge gaps. *Current Pollution Reports*, 5(3), 159-171.
- [61] Nwokolo, S. C., and Ogbulezie, J. C. (2018). A qualitative review of empirical models for estimating diffuse solar radiation from experimental data in Africa. *Renewable and Sustainable Energy Reviews*, 92, 353-393. DOI: <https://doi.org/10.1016/j.rser.2018.04.118>

**Article copyright:** © 2023 Mfongang Erim Agbor, Sunday O. Udo, Igwe O. Ewona, Samuel Chukwujindu Nwokolo, Julie C. Ogbulezie, Solomon Okechukwu Amadi, Utibe Akpan Billy. This is an open access article distributed under the terms of the [Creative Commons Attribution 4.0 International License](https://creativecommons.org/licenses/by/4.0/), which permits unrestricted use and distribution provided the original author and source are credited.

